Representation of Crystallographic Texture using the Symmetric Bingham Distribution

A Thesis

Presented in Partial Fulfillment of the Requirements for the Degree of Bachelor of Science with Honors Research Distinction in the College of Engineering of The Ohio State University

By

Eric Magnuson,

Department of Materials Science and Engineering

The Ohio State University

2016

Thesis Committee:

Dr. Stephen R. Niezgoda, Advisor

Dr. Peter Anderson

Abstract

Crystalline materials often exhibit a strong anisotropy, or directionally dependent response, with respect to their properties. Most structural materials are polycrystalline, composed of many microscopic crystalline regions each with a different orientation with respect to the sample coorrdinate frame. Crystallographic texture, or the presence of a statistically preferred orientation, is a key predictor of macroscale properties and can greatly affect the material response. The estimation of texture from X-ray diffraction data is a classical problem in materials science and geology. Traditional methods for estimating texture have utilized a Fourier series expansion by generalized spherical harmonics. Estimation of texture from discretely sample orientations, via spherical harmonics, requires making several ad-hoc assumptions that can strongly influence the final result.The Bingham distribution, the maximum entropy probability distribution on the space of 3-D rotations (SO(3)), has been proposed as a model distribution for crystallographic texture. However the Bingham distribution does not account for the inherent crystallographic symmetry, so its application has been severely limited. In this work we present a symmetrized Bingham distribution that can be applied to materials with arbitrary symmetries, and efficient numerical scheme for the estimation of distribution parameters from discretely sampled orientation data. We compare texture estimates from discrete orientation data using the symmetrized Bingham model and the classical spherical harmonic technique.

To my family and friends

Acknowledgments

I would like to thank Dr. Stephen Niezgoda for his invaluable assistance and guidance during this process. This work was partially funded by a Undergraduate Research Scholarship provided by the College of Engineering at the Ohio State University.

Vita

Research Experience

Strain Rate Dependent Deformation of Beryllium; Mentors: Dr. Stephen R. Niezgoda (OSU), Dr. Donald W. Brown (Los Alamos National Laboratory) May 2014 - Present

Performed lattice and macroscale measured strain analysis of beryllium using synchrotron data for calibration of crystal plasticity constitutive models

Analyzed crystal texture data from in-situ synchrotron diffraction using MAUD

Development of learning models for crystallographic texture; Mentor: Dr. Stephen R. Niezgoda (OSU) August 2014-Present

Developed optimization procedure to fit analytic statistical distribution to texture components

Applied principles from information theory to learn mixture models for texture from limited data

Publications in Progress

Niezgoda, Stephen R., Magnuson, Eric A., and Jared Glover. Symmetrized Bingham Distribution for Representing Texture: Parameter Estimation with Respect to crystal and Sample Symmetries. Under review for publication in Journal of Applied Crystallography

Field of Study

Materials Science and Engineering

Table of Contents

List of Tables

Table **Page**

List of Figures

Chapter 1: Introduction

Crystallographic texture has a profound impact on materials properties due to the anisotropic properties of real materials. Crystallographic texture is quantified using orientation distribution functions, or ODFs. Typical methods of calculating ODFs rely heavily on applications of spherical harmonics and Fourier series. These methods on ad-hoc assumptions about the texture distribution and consequently are neither statistically rigorous or automatable. The symmetrized Bingham distribution allows rigorous statistical analysis of texture distributions to be conducted for the first time and is capable of being automated.

This thesis first presents a discussion of crystal texture, its origins, and its effects on materials properties. Next, current methods of measuring and analyzing texture are discussed, followed by a description of the mathematics and crystal symmetry, the standard Bingham Distribution, and the symmetrized Bingham distribution. Finally, an expectation-maximation algorithm is developed to estimate parameters for arbitrary crystal textures, and the future applications of this technique are discussed.

Chapter 2: Background

This section of the thesis describes the crystallographic meaning of texture, its origins in sample processing, its effect on materials' properties, and current techniques of measuring and quantifying crystal texture.

2.1 Definition of Crystal Texture

Crystalline materials, which are a significant group of the available engineering materials, are typically organized into small regions of self-consistent crystal lattices, or grains. These grains have well defined crystal structures with coordinate axes used to define lattice positions and planes within the structure, a simple schematic showing crystal orientations is shown below in Figure 2.1. The relationship between the local crystal system (the grain's lattice) and the overall sample geometry is defined as an orientation. In effect, an orientation describes the required rotation necessary to bring the crystal axes into alignment with the sample axes [1].

Orientations are described using several methods, the most prevalent of which are the Euler angles. The Euler angles describe rotations in three-d space using a succession of three rotations around the primary axes of the crystal system. This allows the orientation relationship between an individual grain and the sample frame

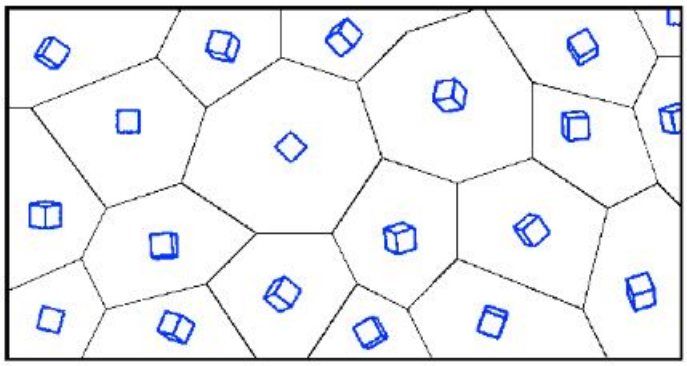

Figure 2.1: Schematic Representation of Crystal Texture, adapted from Rollet

to be completely defined. Alternative methods for describing orientations include the unit rotation matrices, the Bunge angles, and the unit quaternions.

Crystallographic texture is defined as the existence of a preferred crystallographic orientation in a material. An untextured material is composed of grains with random, or near random orientations and the resulting distribution is uniform, or near uniform. By comparison, a heavily textured material features one or more preferred orientations that are concentrated at several multiples of the background texture. Texture distributions are conventionally represented using pole figures, an example of which is shown in Figure 2.2. Each pole figure represents the concentration of the given crystallographic pole, denoted by the appropriate Miller index, in reference to the sample frame.

2.2 Origins of Crystal Texture

The formation of crystallographic texture can be driven by a variety of processes. These driving forces include mechanical deformation, solidification, and recrystallization.

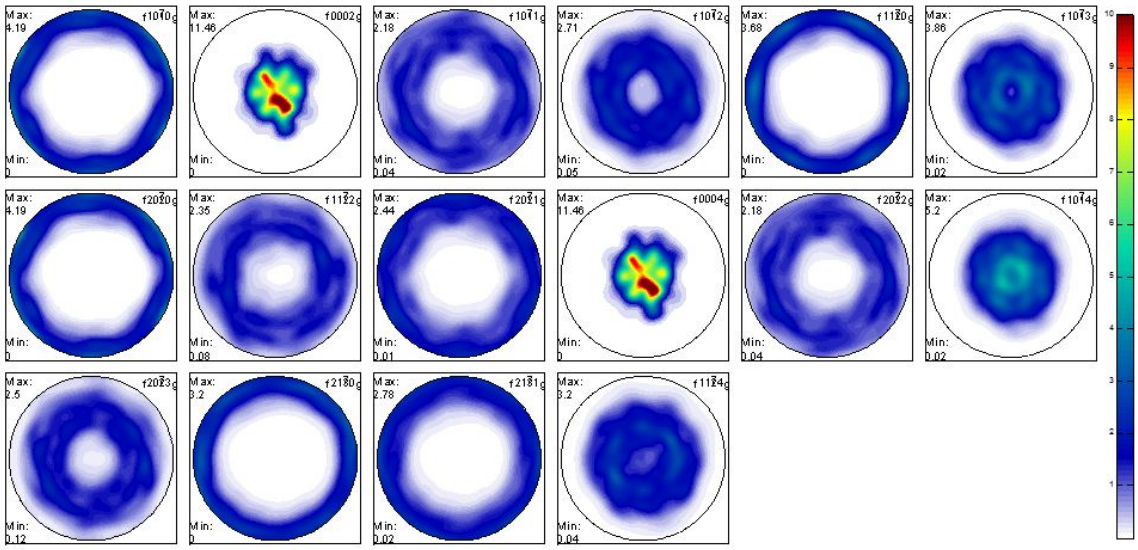

Figure 2.2: X-ray Pole Figures of Material with a Strong Basal Texture

Mechanical deformation of materials, particularly rolling [2] and drawing [3] operations, is one of the primary driving forces for the formation of texture in polycrystalline materials. Deformation driven texture evolution in metals is driven by two competing processes. First, deformation, through the movement of dislocations, can create lattice rotations in the deformed grains [4]. Preferred deformation modes in most materials lead to favored orientations and the development of crystallographic texture. Second, other deformation modes, such as crystal twinning, also create large scale changes in the orientation distribution within a sample. In particular, deformation twinning creates a large change in texture during the deformation of materials [5].

Solidification, and the associated phase transformations, can also lead to the formation of crystallographic texture [6]. For example, processing of titanium can result in several different texture distributions for the same alloy. In particular, the preferred

orientation is different for both the α and β phases. The mixture of these phases varies due to processing, which can lead to large differences in texture between samples.

Recrystallization of deformed materials also leads to texture evolution in metals [7]. The recrystallization texture of a material is dependent on several factors. The heat treatment of the material can lead to different textures or a randomly oriented material. Second, the degree of cold work applied to the material can lead to different textures in the annealed materials. Third, the starting texture can also affect the final texture [8].

2.3 Texture Induced Anisotropy of Properties

Crystallographic texture can have a dramatic effect on materials' properties. The following section discusses the effects of crystallographic texture on two materials systems; mechanical properties drawn aluminum sheet and superconducting properties in YBCO ceramics.

2.3.1 Anisotropy of Mechanical Properties

Crystallographic texture can create large anisotropy in the mechanical properties of crystalline solids. Single crystals of material generally feature large anisotropy in mechanical properties dependent on the direction of applied stress [9]. This results in differences in both the elastic and plastic response in the material. One example of this is the deep drawing of metals, a process often used for the production of containers.

Most sheet materials are produced by rolling. The rolling process creates a strong texture in the final material, which is dependent on the crystal structure of the material [10]. For example, rolled Mg alloys typically have a strong basal texture [11],

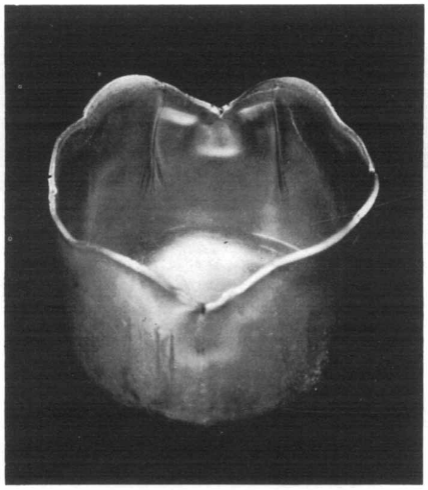

Figure 2.3: Deep drawn Al showing earing, reproduced from Tucker [14]

with varying degrees of intensity. In Mg, this basal texture results in a significant portion of C-axes pointing towards the sample's normal direction. As a result of the HCP structure of Mg, the basal texture limits plasticity along the normal direction of the sample due to the higher critical resolved shear stress to initiate pyramidal slip in this system [12].

Texture induced anistropy is also a concern in aluminum alloys. Aluminum alloys, like Al 3004, commonly develop strong rolling textures during cold rolling [13]. As in magnesium alloys, this results in strong plastic anisotropy in the final material. For example, during deep drawing, heavily rolled sheet stock typically undergoes earing, as shown in Figure 2.3. This creates waste material, increasing costs for the manufacturer. The texture of the starting material, and the degree of anisotropy, have an important effect on the properties of the material [14].

2.3.2 Anisotropy of Electrical Properties in Superconductors

Crystallographic texture is also an area of concern in high temperature superconductors, particularly the YBCO superconducting systems.The YBCO (Yttrium-Barium-Copper-Oxide) system is a non-stoichiometric ceramic oxide that displays a high superconductivity transition temperature at 87K [15]. The high temperature superconductivity of YBCO is significantly affected by the crystallographic texture of the sample.

YBCO is a modified perovskite structure, as shown in Figure 2.4. The copper containing crystallographic planes are responsible for superconduction in this material. However, in bulk YBCO, misalignment of these crystallographic planes results in loss of superconductivity in the bulk material, which has limited the commercial utility of this class of materials [16]. Methods of controlling texture development in YBCO have focused on the production of epitaxial films deposited on metallic substrates[17]. These methods allow for alignment of the superconducting planes in YBCO, controlling the texture, and also produce a flexible superconducting film, usable in engineering applications.

2.4 Current Methods of Texture Measurement and Analysis

Texture measurement and analysis in materials has been focused on two specific areas: macrotexture and microtexture. Macrotexture methods focus on the average crystallographic texture throughout the entire sample while microtexture measurements focus on discrete orientations over a more limited region of sample.

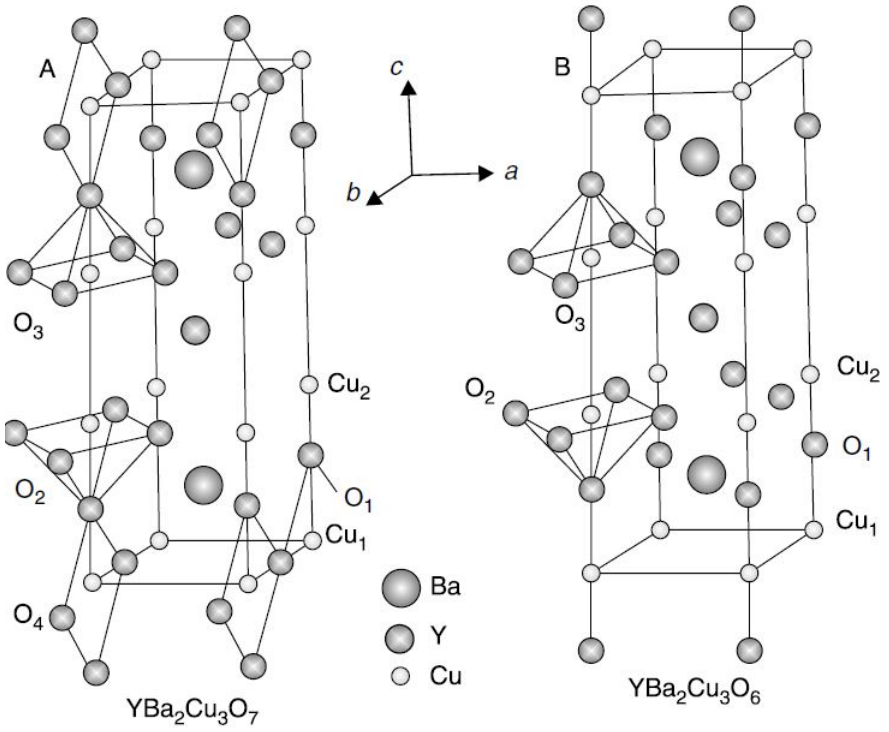

Figure 2.4: YBCO Structure, reproduced from Saxena [18]

2.4.1 Bulk Texture Measurements

Bulk texture measurements, which focus on average crystallographic orientations throughout the entire sample, are typcically gathered using bulk diffraction measurements, either with neutrons or synchrotron x-rays. Neutron scattering techniques allow the direct measurement of crystal texture, typically using large diffractometers, by measuring diffraction patterns from several banks of time-of-flight diffractometers [19]. Analysis of neutron texture measurements is typically conducting using full pattern Rietveld refinements, which require experience to correctly fit the texture distribution and avoid local minima.

Bulk texture measurements are also taken using synchrotron radiation. The sample is illuminated by a high energy, high flux x-ray beam and 2-d diffraction patterns are taken. The sample is rotated to illuminate different grains within the sample, produced several diffraction patterns. These are then integrated to produce an array of 1-d spectra. The analysis then proceeds in the same manner as the neutron diffraction measurements, with full-pattern analysis using the Rietveld method and fitting of the orientation data with spherical harmonics [20].

2.4.2 Micro Texture Measurements

Unlike bulk texture measurements, which measure the average orienation across the entire sample, micro-texture measurements focus on determining the orientations of a smaller number of discrete grains in the sample. Microtexture measurements are typically conducted using electron backscatter diffraction (EBSD) or high energy diffraction microscopy (HEDM).

EBSD measurements are conducted using a specialized camera in the scanning electron microscope. The sample is tilted within the SEM and then the electron beam is focused on the sample. A fraction of the electrons diffract out of the sample and are indexed by the EBSD camera. This forms diffraction patterns which may then be used to determine the orientation and crystal structure of that region of the sample [21]. An orientation map of the sample is then developed by indexing the diffraction patterns with a lookup table. This technique allows the mapping of discrete orientations rapidly with relatively small capital investment in equipment [22].

The recently developed technique of high energy diffraction microscopy (HEDM) offers the promise of resolving microstructure and orientation data without the need to section samples, as in EBSD [23]. The sample, typically composed of several dozen grains is illuminated by a high energy electron beam, typically produced by a synchrotron storage ring, and rotated in the beam to produce an array of diffraction patterns. By selectively illuminating individual grains within the sample, their orientation, location, and relative size may be indexed. This allows the microstructure of the sample to be reconstructed and analyzed without the need for destructive testing [24]. However, analysis of HEDM data is computationally expensive and the required equipment, a synchrotron storage ring and associated equipment, requires a large investment in capital and maintenance.

2.4.3 Analysis of Texture Measurements

Texture analysis methods have been traditionally focused on bulk texture measurements, typically obtained through x-ray diffraction. Analysis of integrated 1-d

spectra is typically conducted by the Rietveld method, a least squares method that fits the entire spectra profile [25]. The ODF is then typically generated using the spherical harmonic method described by Bunge [26].

The spherical harmonic method is also generally applied to the analysis of micro-texture; however, it is not well-suited to this task. The spherical harmonic method requires ad-hoc assumptions about the parameters of the ODF, which has several consequences for the analysis. First, the spherical harmonic method is not easily automated. Texture analysis using this method requires supervision and careful refinement to avoid local minima. Second, the required assumptions about the texture distribution do not allow rigorous statistical analysis of micro-texture distributions. The symmetric Bingham distribution method promises to solve both of the problems with traditional analysis of micro-texture [27].

Chapter 3: The Standard Bingham Distribution

3.1 Definition of the Bingham Distribution

The Bingham distribution is a probability distribution defined over the n-d hypersphere [28]. In the case where n=4, the Bingham distribution is defined over the unit quaternions and can be written as shown in Equation (3.1). The unit quaternions are isomorphic to the unit rotations used to describe crystallographic orientations, so the Bingham distribution is suitable for the representation of crystallographic texture [27].

$$p(\mathbf{g}; \mathbf{\Lambda}, \mathbf{V}) = \frac{1}{F(\mathbf{\Lambda})} \exp \sum_{i=1}^{4} \lambda_i (\mathbf{v}_i \cdot \mathbf{g})^2 \tag{3.1}$$

The Bingham distribution represents the probability p of a given orientation, $\mathbf{g}$, in a distribution defined by the parameters $\mathbf{\Lambda}$, a 4-vector representing the concentration of the distribution along the primary directions, F, a normalization constant parametrized by $\mathbf{\Lambda}$, and $\mathbf{V}$, a 4×4 matrix composed of 4 unit quaternions representing the principal directions of the distribution. The primary difficulty in the computation of the Bingham distribution lies in the normalization constant F, which is a hypergeometric function of matrix argument [28]. The normalization constant is difficult to compute in real time. As a result, the normalization constant is calculated using

a lookup table of precomputed values of F with interpolation for arbitrary values of $\mathbf{\Lambda}$ [29].

The parameters of the standard Bingham distribution may be determined using closed form maximimum likelihood estimators for both $\mathbf{\Lambda}$ and $\mathbf{V}$, which are respectively designated $\hat{\mathbf{\Lambda}}$ and $\hat{\mathbf{V}}$. For a set of N orientations, $\mathcal{G} = \{\mathbf{g}^{(1)}, \ldots, \mathbf{g}^{(N)}\}$, the scatter matrix S can be written as shown below.

$$\mathbf{S} = \frac{1}{N} \sum_{i=1}^{n} \mathbf{g}^{(i)} \mathbf{g}^{(i)^T} = E\{\mathbf{g}\mathbf{g}^T\} \tag{3.2}$$

The scatter matrix can then be used to estimate the MLEs for both $\mathbf{\Lambda}$ and $\mathbf{V}$ utilizing an eigenvalue decomposition of S. The eigenvectors corresponding to the second, third, and fourth eigenvalues correspond to the columns of $\mathbf{V}$. The elements of $\mathbf{\Lambda}$ may then be calculated by setting the derivative of the log-likelihood of the distribution equal to zero, resulting in the equation shown below. The derivatives of the normalization constant are also stored in a precomputed lookup table, allowing rapid computation of the derivatives via interpolation. [27]

$$\frac{1}{F(\mathbf{\Lambda})} \frac{\partial F(\mathbf{\Lambda})}{\partial \lambda_j} = \mathbf{v}_j^T \mathbf{S} \mathbf{v}_j. \tag{3.3}$$

The closed form MLEs for the unsymmetrized Bingham distribution allow rapid computation of parameters for arbitrary Bingham distributions when combined with the precomputed normalization constants developed by Glover.

3.2 Current Applications and Limitations of the Standard Bingham Distribution

The Bingham distribution was first used to describe crystallographic texture by Schaeben [30] and Kunze [31]. They applied the Bingham distribution to the modelling of texture components, including fibers and sheets. The unsymmetrized Bingham distribution is useful in the modelling of unimodal textures, but more complex textures require mixtures of Bingham distributions for accurate representation. Furthermore, the Bingham distribution also has applications in machine vision [32].

The applications of the Bingham distribution to crystallographic texture have been limited for several reasons. First, the normalization constant is computationally expensive to compute on demand. This issue has been solved by the creation of lookup tables for both the normalization constant and its derivatives. Second, the standard Bingham distribution does not account for inherent crystal symmetry or processing induced sample symmetry. Consequently, the standard Bingham distribution has been limited to triclinic crystal systems with no processing induced sample symmetry. The systems are not representative of real engineering materials, so the overall utility of the Bingham distribution to texture analysis has been limited.

Chapter 4: The Symmetrized Bingham Distribution

As described previously, the standard Bingham distribution does not account for either crystal or sample symmetry, limiting its utility in texture analysis. We have developed a new variant of the Bingham distribution applicable to systems with arbitrary crystal and sample symmetry.

4.1 Distribution Invariance under Symmetry Operations

Extension of the Bingham Distribution to symmetric materials requires the proposed distribution to be invariant under sample and crystal symmetry. First, consider the group $\mathcal{G} = \{\mathbf{G}_1, ..., \mathbf{G}_M\}$, with a finite number of elements, each of which acts on the space $\mathcal{X}$ where each element $\mathcal{G}_i$ maps $\mathcal{X} \rightarrow \mathcal{X}$. Elements of $\mathcal{G}$ are associative, with inverse and identity operations [33]. A function, $f(x)$, is considered invariant under $\mathcal{G}$ if $f(Gx) = f(x)$ for $G \in \mathcal{G}$. Next, we consider a random variable $\mathbf{X}$ defined on $\mathcal{X}$. The probability distribution of $\mathbf{x}$ obeys the following theorem.

Theorem: The probability density function, $f(x)$ is invariant under $\mathcal{G}$ if and only if

$\mathbf{f(x)} = \frac{\mathbf{1}}{\mathbf{M}} \sum_{\mathbf{i=1}}^{\mathbf{M}} \mathbf{f(G_i x)}$

Proof. If the above theorem holds true, then $f(Gx) = M^{-}1 \sum_{i=1}^{M} f(G_i G x)$. $\mathcal{G}$ is a group where $\mathcal{G}G = \mathcal{G}$, so $M^{-}1 \sum_{i=1}^{M} f(G_i G x) = M^{-}1 \sum_{i=1}^{M} f(G_j x)$ and $f(x) = f(Gx)$. Alternatively, if $f(Gx) = f(x)$ then $M^{-}1 \sum_{i=1}^{M} f(G_i x) = M^{-}1 \sum_{i=1}^{M} f(x) = f(x)$. $\square$

In effect, the above theorem states that any probability distribution that is invariant under a group can be represented as a mixture of translated distributions under the group. This simplifies the estimation of parameters for distributions with spherical symmetry components [34].

4.2 The Symmetrized Bingham Distribution

In order to practically apply the Bingham distribution to ODF representation we need to account for the underlying crystallographic and sample symmetries of the material and processing operations. Let $\mathcal{Q}^{\mathrm{c}} = \{\mathbf{q}_1^{\mathrm{c}}, \ldots \mathbf{q}_M^{\mathrm{c}}\}$ denote a group whose elements transform one orientation to a crystallography equivalent one.

If $\mathbf{q}^{\mathrm{c}} \in \mathcal{Q}^{\mathrm{c}}$ then any function where $f(\mathbf{q}^{\mathrm{c}} * \mathbf{g}) = f(\mathbf{g})$ is said to be invariant under $\mathcal{Q}^{\mathrm{c}}$. A material sample can also contain statistical symmetry due to processing. The classic example is a statistical two-fold rotation axis about the rolling, transverse, and normal directions of a rolled plate resulting in orthotropic sample symmetry [35]. The sample symmetry group $\mathcal{Q}^{\mathrm{s}} = \{\mathbf{q}_1^{\mathrm{s}}, \ldots, \mathbf{q}_P^{\mathrm{s}}\}$ is defined in an identical way to the crystal symmetry group except the group operation is right multiplication.

For materials with both symmetries any function of $\mathbf{g}$ must be invariant under both symmetries as [36],

$$f(\mathbf{q}^{\mathrm{c}} * \mathbf{g} * \mathbf{q}^{\mathrm{s}}) = f(\mathbf{g}). \tag{4.1}$$

As discussed previously, Chen recently derived the required form for symmetry invariant probability distributiosn [34]. Here we trivially extend their result to include

sample symmetry and state that the density function $p : SO(3) \rightarrow R$ is jointly invariant under $\mathcal{Q}^{\mathrm{c}}$ and $\mathcal{Q}^{\mathrm{s}}$ if and only if

$$p(\mathbf{g};\boldsymbol{\Theta}) = \frac{1}{M}\frac{1}{P}\sum_{i=1}^{M}\sum_{j=1}^{P} p(\mathbf{q}_i^{\mathrm{c}} * \mathbf{g} * \mathbf{q}_j^{\mathrm{s}};\boldsymbol{\Theta}) \tag{4.2}$$

where $\boldsymbol{\Theta}$ are the parameters of the probability density. Eq. 4.2 states that any probability density $p(\mathbf{g})$ over the orientations which is invariant to crystallographic and sample symmetry can be represented as a finite mixture with equal weights of the rotated density under the combined crystallographic and sample symmetry groups actions.

$$p(\mathbf{g};\mathcal{Q},\boldsymbol{\Lambda},\mathbf{V}) = \frac{1}{MP}\sum_{i=1}^{M}\sum_{j=1}^{P} p(\mathbf{q}_i^{\mathrm{c}} * \mathbf{g} * \mathbf{q}^{\mathrm{s}};\boldsymbol{\Lambda},\mathbf{V}) \tag{4.3}$$

$$= \frac{1}{MP}\sum_{i=1}^{M}\sum_{j=1}^{P} p(\mathbf{g};\boldsymbol{\Lambda},\mathbf{Q}_i^{\mathrm{c}}\mathbf{V}\mathbf{Q}_j^{\mathrm{s}}) = \frac{1}{MP}\sum_{i=1}^{M}\sum_{j=1}^{P} p(\mathbf{g};\boldsymbol{\Lambda},\mathbf{V}_{ij}) \tag{4.4}$$

$$= \frac{1}{MP}\frac{1}{F(\boldsymbol{\Lambda})}\sum_{i=1}^{M}\sum_{j=1}^{P}\left[\exp\sum_{k=1}^{4}\lambda_i\left([\mathbf{V}_{ij}]_k\cdot\mathbf{g}\right)^2\right] \tag{4.5}$$

where $\mathcal{Q}$ denotes the symmetry groups, $\mathbf{Q}_r$ denotes the quaternionic matrix where the product $\mathbf{Q}_r\mathbf{V}$ is equivalent to applying rotation $\mathbf{q}_r$ to each column of $\mathbf{V}$, and $[\mathbf{V}_{ij}]_k$ denotes the kth column of V_{ij}. Going from eq. 4.3 to eq. 4.4 requires the application of the inner quaternion product $\mathbf{v}_k \cdot \mathbf{g}$ in eq. 3.1 and the observation that the inverse of symmetry elements must also be elements of the symmetry group. EQ. 4.3 states that the symmetrized Bingham distribution is a finite mixture of the standard quaternion Bingham distributions, with each component a) having equal weight b) having principal directions rotated by $\mathbf{Q}_i^{\mathrm{c}}\mathbf{V}\mathbf{Q}_j^{\mathrm{s}} = \mathbf{V}_{ij}$ and c) having the same concentration parameters $\boldsymbol{\Lambda}$. A similar weighted mixture mixture was defined in [37] and termed the Pseudo-Bingham distribution.

Given set $\mathcal{G}$ containing N orientation measurements, the data log-likelihood is given by

$$\ln p(\mathcal{G}; \mathbf{\Lambda}, \mathbf{V}) = -N \ln \left(MPF(\mathbf{\Lambda}) \right) + \sum_{n=1}^{N} \ln \sum_{i=1}^{M} \sum_{j=1}^{P} \exp \left(\sum_{k=1}^{4} \lambda_k \left([\mathbf{V}_{ij}]_k \cdot \mathbf{g}_n \right)^2 \right) \tag{4.6}$$

4.3 Limitations on the Utility of the Symmetrized Distribution

The symmetric Bingham distribution solves several of the problems with the standard, unsymmetrized Bingham distribution; however, the inclusion of sample and crystal symmetry destroys the closed form solution to the MLEs for the Bingham parameters. Furthermore, while the derivatives of the symmetrized distribution are well defined and trivial to compute, estimating the parameters of the distribution with a gradient descent is computationally expensive and difficult due to local minima in the derivatives of the distribution.

Chapter 5: EM-ML Estimation of Symmetric Bingham Parameters

5.1 EM-ML Algorithm

As mentioned earlier, $\mathbf{S}$ is a sufficient statistic for parameter estimation for the standard Bingham distribution. Eq. 4.4 shows that the symmetrized Bingham is finite mixture of rotated standard Bingham distributions. If $\mathbf{S}$ could be calculated for the symmetrized case the standard ML estimates $\hat{\mathbf{\Lambda}}$ and $\hat{\mathbf{V}}$ could be trivially computed. Consider a set of N discrete orientations, $\mathcal{G} = \{\mathbf{g}^{(1)}, \ldots, \mathbf{g}^{(N)}\}$ which was generated by sampling a symmetrized Bingham distribution. In order to calculate $\mathbf{S}$ we are missing information. The complete dataset would also contain a label which identifies which of the MP rotated components of the mixture generated each sample [**niezgoda2013**, 34, 38]. The EM-ML algorithm seeks the Bingham ODF which maximizes the probability of measuring the orientation data by a) estimating the labels given an estimate of the Bingham parameters (E-step) then b) using this new estimate of the labels to update the Bingham parameters (M-step). The algorithm is described more formally below.

For compactness let $\Theta = \{\mathcal{Q}, \mathbf{\Lambda}, \mathbf{V}\}$ denote the complete set of parameters necessary to specify the symmetrized Bingham $p(\mathbf{g}; \Theta)$. Further let $\theta_{ij} = \{\mathbf{\Lambda}, \mathbf{V}_{ij} = \mathbf{Q}_i^c \mathbf{V} \mathbf{Q}_j^s\}$ denote the set of parameters necessary to specify an individual rotated

component of the mixture, $p(\mathbf{g};\theta_{ij})$. Define a set of binary label vectors $\mathcal{Z} = \left[\mathbf{z}^{(1)},\ldots,\mathbf{z}^{(N)}\right]$, where the elements of each vector $z_{ij}^{(n)}$ take the value 1 if $\mathbf{g}^{(n)}$ was generated by $p(\mathbf{g};\theta_{ij})$ and 0 otherwise. If $\mathcal{Z}$ could be measured, then computing the scatter matrix and finding the ML estimate of the parameters $\hat{\Theta}$ would be trivial.

The complete data log-likelihood is given by

$$\log p(\mathcal{G},\mathcal{Z};\Theta) = \frac{1}{MP}\sum_{n=1}^{N}\sum_{i=1}^{M}\sum_{j=1}^{P} z_{ij}^{(n)} \log p(g^{(n)};\theta_{ij}). \tag{5.1}$$

An ideal algorithm would maximize eq. 5.1 directly. However optimization of functions of binary variables (i.e. $\mathcal{Z}$) is problematic [39]. Instead we define the conditional expectation, $\mathcal{W} = E\left[\mathcal{Z}|\mathcal{G},\hat{\Theta}\right]$. $w_{ij}^{(n)}$ gives the probability that $z_{ij}^{(n)} = 1$ or equivalently the probability that orientation $\mathbf{g}^{(n)}$ was generated by the rotated Bingham $p(\mathbf{g};\theta_{ij})$. By substituting $\mathcal{W}$ into eq. 5.1 we can use Bayes rule to update the probabilities of mixture assignments. In the EM literature this is termed the Q function. If $\hat{\Theta}$ represents a current estimate of the parameters then

$$\begin{aligned} Q(\Theta|\hat{\Theta}) &= E\left[\log p(\mathcal{G},\mathcal{Z}|\Theta)|\mathcal{G},\hat{\Theta}\right] \\ &= \log p(\mathcal{G},\mathcal{W}|\Theta) \end{aligned} \tag{5.2}$$

The E-step consists of using Bayes rule to update $\mathcal{W}$ as

$$\begin{aligned} w_{ij}^{(n)} &= E[z_{ij}^{(n)}|\mathcal{G},\hat{\Theta}] = \mathcal{P}[z_{ij}^{(n)} = 1|\mathbf{g}^{(n)},\hat{\Theta}] \\ &= \frac{(MP)^{-1}p(\mathbf{g}^{(n)};\hat{\theta}_{ij})}{\sum_{s,t}(MP)^{-1}p(\mathbf{g}^{(n)};\hat{\theta}_{st})}. \end{aligned} \tag{5.3}$$

Then in the M-step the parameter estimates $\hat{\Theta}$ are updated to maximize eq. 5.2. The ML estimate for $Q(\Theta|\hat{\Theta})$ can then be derived, by setting the derivatives with respect to the parameters to zero and solving. The ML estimates take exactly the same form

as those given for the standard Bingham if the scatter matrix is replaced by $\mathbf{S}(\mathcal{Q})$ the symmetrized scatter matrix

$$\mathbf{S}(\mathcal{Q}) = \frac{1}{N}\sum_{n=1}^{N}\sum_{i=1}^{M}\sum_{j=1}^{P} w_{ij}^{(n)}\mathbf{g}_{ij}^{(n)}\mathbf{g}_{ij}^{(n)^T} \tag{5.4}$$

where $\mathbf{g}_{ij}^{(n)} = (\mathbf{q}_i^{\mathrm{s}})^{-1} * \mathbf{g}^{(n)} * (\mathbf{q}_j^{\mathrm{c}})^{-1}$. The EM-ML algorithm alternates between eq. 5.3 and eq. 5.4 until convergence is reached. For this work convergence was defined as the change in eq. 5.2 between iterations was less than some small value , $\Delta Q(\Theta|\hat{\Theta})/n \leq \delta$.

5.2 Estimation of Strong Textures

We applied the algorithm to the case of texture estimation in a cubic-orthorhombic material, meaning that each orientation has 96 symmetric equivalents (the composition of 24 from cubic crystallographic Laue class $m\bar{3}m$ and 4 from sample symmetry group). $n = 1000$ i.i.d. sample orientations, and the stopping criterion $\delta = 10^{-5}$ was used. In order to define a "ground-truth" for comparison, n quaternions were sampled from a non-symmetrized Bingham distribution with known parameters. The ML estimates of the quaternion Bingham parameters (Eqs. 3.2 and 3.3) were computed from the samples and the resulting fit Bingham was used as the ground truth. The sampled quaternions were each replaced with a randomly chosen symmetrically equivalent orientation to produce $\mathcal{G}$. In this way we ensured direct comparison between the EM-ML process to fit the symmetrized Bingham and the ML estimates of the standard quaternion Bingham distribution using equivalent initial data. The quality of fit was evaluated by computing the data log likelihood (Eq. 4.6) and the texture entropy for each ODF as well as the integrated error between the fit ODF and the ground truth.

Table 5.1: Comparison of ground truth versus fit symmetrized Bingham ODF for a strongly textured distribution.

	Λ	Log Likelihood	Integrated Error	Entropy
Initial Target	[-25.00 -20.00 -15.00]	181.63	0.0281	-0.1926
Ground Truth	[-24.98 -19.11 -15.46]	182.23	0.000	-0.2058
Fit Symmetric	[-24.76 -18.79 -15.80]	183.45	0.0096	-0.2027

Figure 5.1 shows the results of this procedure. For convenience the ODFs are plotted with respect to the Bunge-Euler angles at constant ϕ_2 sections, for interpretation of the ODF images see [36, 35]. 1000 samples were drawn from an anisotropic Bingham distribution with $\Lambda = [-25, -20, -15]$ and V chosen as a random orthogonal matrix. As expected the fit ODF is virtually identical to the ground truth ODF. Specific details of the goodness of the fit are given in Table 5.1. It is interesting to note that the likelihood of the symmetrized fit is slightly larger than the ground truth fit. Additionally the progression of the algorithm, shown by the evolution of $Q(\Theta|\hat{\Theta})$ with each iteration, is highlighted in Figure 5.2 .

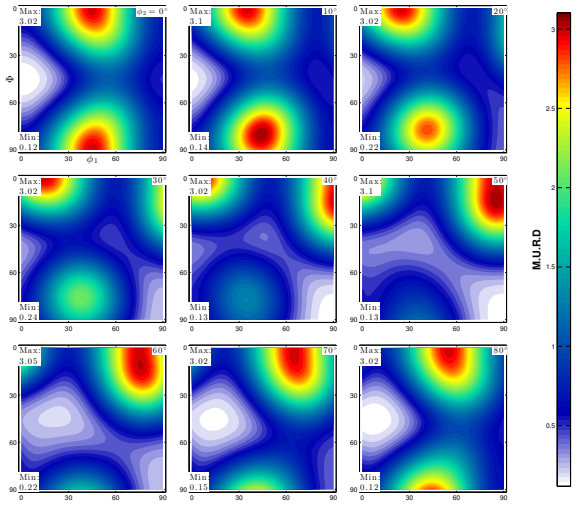

(a)

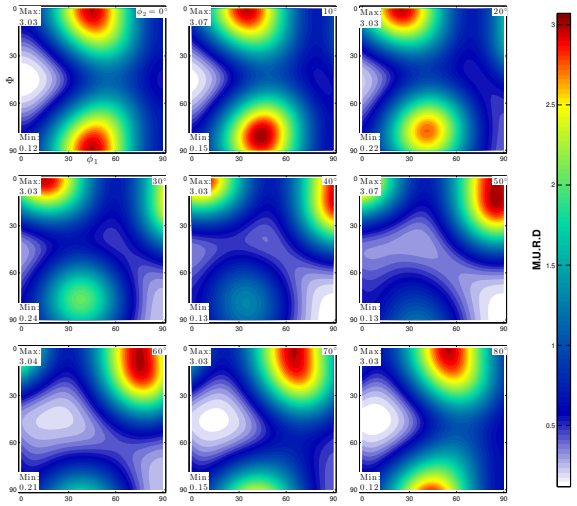

(b)

Figure 5.1: Comparison of the ground truth ODF (a) against the fit ODF for a material with cubic crystal symmetry and orthotropic sample symmetry. For convenience the ODFs are plotted as ϕ_2 sections of the Bunge-Euler angles [36], as is routinely done in the quantitative texture analysis literature.

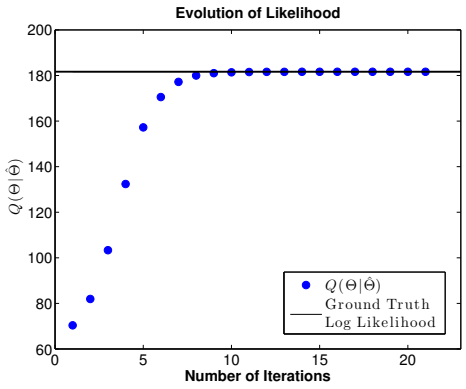

Figure 5.2: Comparison of ground truth versus fit symmetrized Bingham ODF for strongly textured distribution

Chapter 6: Conclusions and Future Applications

As demonstrated, the symmetrized Bingham distribution is a promising method for performing rigorous statistical analysis of discrete crystallographic data. The previous limitations in estimating the parameters of the symmetrized Bingham distribution have been eliminated through the development of an expectation-maximization algorithm. This method avoids the a priori assumptions required for the traditional spherical harmonic technique proposed by Bunge.

In the future, the symmetric Bingham distribution will be incorporated into a mixture model combined with an unsupervised learning algorithm. This will allow more rapid fitting of ODFs to discrete crystallographic data and allow increased automation of this process. Furthermore, the symmetrized Bingham distribution allows rigorous statistical analysis of crystallographic data that has not been previously possible. This will allow detailed analysis of crystallographic texture and their effects on materials properties.

Bibliography

[1] U. F. Kocks, C. N. Tomé, and H. R. Wenk. *Texture and Anisotropy: Preferred Orientations in Polycrystals and Their Effect on Materials Properties*. Cambridge University Press, 2000, p. 676. ISBN: 052179420X. DOI: 10.2277/052179420X.

[2] J Grewen. "Textures of Hexagonal Metals and Alloys and Their Influence on Industrial Application". In: *Pont-a-Mousson Conference on Texture* (1973).

[3] A.T. English and G.Y. Chin. "On the variation of wire texture with stacking fault energy in f.c.c. metals and alloys". In: *Acta Metallurgica* 13.9 (1965), pp. 1013–1016. ISSN: 00016160. DOI: 10.1016/0001-6160(65)90010-6.

[4] L Margulies, G Winther, and H F Poulsen. "In situ measurement of grain rotation during deformation of polycrystals." en. In: *Science (New York, N.Y.)* 291.5512 (2001), pp. 2392–4. ISSN: 0036-8075. DOI: 10.1126/science.1057956. URL: http://science.sciencemag.org/content/291/5512/2392.abstract.

[5] W. Heye and G. Wasserman. "The formation of the rolling textures in FCC metals by slip and twinning". In: *Scripta Metallurgica* 2.4 (1968), pp. 205–207. ISSN: 00369748. DOI: 10.1016/0036-9748(68)90228-7. URL: http://www.sciencedirect.com/science/article/pii/0036974868902287.

[6] P.A Kobryn and S.L Semiatin. "Microstructure and texture evolution during solidification processing of Ti6Al4V". In: *Journal of Materials Processing Technology* 135.2-3 (2003), pp. 330–339. ISSN: 09240136. DOI: 10.1016/S0924-0136(02)00865-8. URL: http://www.sciencedirect.com/science/article/pii/S0924013602008658.

[7] Roger D. Doherty. "Recrystallization and texture". In: *Progress in Materials Science* 42.1-4 (1997), pp. 39–58. ISSN: 00796425. DOI: 10.1016/S0079-6425(97)00007-8. URL: http://www.sciencedirect.com/science/article/pii/S0079642597000078.

[8] Y.B. Park, D.N. Lee, and G. Gottstein. "The evolution of recrystallization textures in body centred cubic metals". In: *Acta Materialia* 46.10 (1998), pp. 3371–3379. ISSN: 13596454. DOI: 10.1016/S1359-6454(98)00052-4. URL: http://www.sciencedirect.com/science/article/pii/S1359645498000524.

[9] Richard W. Hertzberg. *Deformation and fracture mechanics of engineering materials*. J. Wiley & Sons, 1996, p. 786. ISBN: 0471012149.

[10] Krzysztof Wierzbanowski. "Computer simulation of rolling texture formation in H.C.P. and orthorhombic metals". In: *Scripta Metallurgica* 13.9 (1979), pp. 795–799. ISSN: 00369748. DOI: 10.1016/0036-9748(79)90161-3.

[11] Sangbong Yi et al. "Mechanical anisotropy and deep drawing behaviour of AZ31 and ZE10 magnesium alloy sheets". In: *Acta Materialia* 58.2 (2010), pp. 592–605. ISSN: 13596454. DOI: 10.1016/j.actamat.2009.09.038.

[12] Yizhe Tang and Jaafar A. El-Awady. "Formation and slip of pyramidal dislocations in hexagonal close-packed magnesium single crystals". In: *Acta Materialia* 71 (2014), pp. 319–332. ISSN: 13596454. DOI: 10.1016/j.actamat.2014.03.022.

[13] P. A. Hollinshead and T. Sheppard. "Development of rolling textures in aluminum alloy 3004 subjected to varying hot-rolling deformation". In: *Metallurgical Transactions A* 20.8 (1989), pp. 1495–1507. ISSN: 0360-2133. DOI: 10.1007/BF02665506.

[14] G.E.G Tucker. "Texture and earing in deep drawing of aluminium". In: *Acta Metallurgica* 9.4 (1961), pp. 275–286. ISSN: 00016160. DOI: 10.1016/0001-6160(61)90220-6.

[15] M. K. Wu et al. "Superconductivity at 93 K in a new mixed-phase Y-Ba-Cu-O compound system at ambient pressure". In: *Physical Review Letters* 58.9 (1987), pp. 908–910. ISSN: 0031-9007. DOI: 10.1103/PhysRevLett.58.908.

[16] Gernot Krabbes et al. *High Temperature Superconductor Bulk Materials: Fundamentals, Processing, Properties Control, Application Aspects*. John Wiley & Sons, 2006, p. 311. ISBN: 3527607412.

[17] A. Goyal et al. "High critical current density superconducting tapes by epitaxial deposition of YBa2Cu3Ox thick films on biaxially textured metals". In: *Applied Physics Letters* 69.12 (1996), p. 1795. ISSN: 00036951. DOI: 10.1063/1.117489.

[18] Ajay Kumar Saxena. *High-Temperature Superconductors*. Springer Science & Business Media, 2009, p. 238. ISBN: 3642007120.

[19] SC Vogel and C Hartig. "Texture measurements using the new neutron diffractometer HIPPO and their analysis using the Rietveld method". In: *Powder ...* (2004).

[20] L. Lutterotti et al. "Texture, residual stress and structural analysis of thin films using a combined X-ray analysis". In: *Thin Solid Films* 450.1 (2004), pp. 34–41. ISSN: 00406090. DOI: 10.1016/j.tsf.2003.10.150.

[21] Stuart I Wright et al. "Electron imaging with an EBSD detector." In: *Ultramicroscopy* 148 (2015), pp. 132–45. ISSN: 1879-2723. DOI: 10.1016/j.ultramic.2014.10.002.

[22] Peter J. Goodhew, John Humphreys, and Richard Beanland. *Electron Microscopy and Analysis, Third Edition*. Vol. 30. CRC Press, 2000, p. 254. ISBN: 0748409688.

[23] U. Lienert et al. "High-energy diffraction microscopy at the advanced photon source". In: *JOM* 63.7 (2011), pp. 70–77. ISSN: 1047-4838. DOI: 10.1007/s11837-011-0116-0.

[24] J. V. Bernier et al. "Far-field high-energy diffraction microscopy: a tool for intergranular orientation and strain analysis". In: *The Journal of Strain Analysis for Engineering Design* 46.7 (2011), pp. 527–547. ISSN: 0309-3247. DOI: 10.1177/0309324711405761.

[25] H. M. Rietveld. "A profile refinement method for nuclear and magnetic structures". EN. In: *Journal of Applied Crystallography* 2.2 (1969), pp. 65–71. ISSN: 00218898. DOI: 10.1107/S0021889869006558.

[26] H.-J. Bunge. *Texture Analysis in Materials Science: Mathematical Methods*. Elsevier, 2013, p. 614. ISBN: 1483278395.

[27] Stephen R. Niezgoda and Jared Glover. "Unsupervised Learning for Efficient Texture Estimation From Limited Discrete Orientation Data". In: *Metallurgical and Materials Transactions A* 44.11 (2013), pp. 4891–4905. ISSN: 1073-5623. DOI: 10.1007/s11661-013-1653-7.

[28] Christopher H Bingham. *An Antipodally Symmetric Distribution on the Sphere*. 1974. (Visited on 03/29/2016).

[29] Jared Glover, Gary Bradski, and Radu Bogdan Rusu. "Monte carlo pose estimation with quaternion kernels and the bingham distribution". In: *Robotics: science and systems*. Vol. 7. 2012, p. 97.

[30] H. Schaeben. "Texture Approximation or Texture Modelling with Components Represented by the von MisesFisher Matrix Distribution on SO (3) and the Bingham Distribution on S 4+ +". EN. In: *Journal of Applied Crystallography* 29.5 (1996), pp. 516–525. ISSN: 0021-8898. DOI: 10.1107/S0021889896002804.

[31] Karsten Kunze and Helmut Schaeben. "The Bingham Distribution of Quaternions and Its Spherical Radon Transform in Texture Analysis". In: *Mathematical Geology* 36.8 (2004), pp. 917–943. ISSN: 0882-8121. DOI: 10.1023/B:MATG.0000048799.56445.59.

[32] Andrea Fusiello, Vittorio Murino, and Rita Cucchiara, eds. *Computer Vision ECCV 2012. Workshops and Demonstrations*. Vol. 7584. Lecture Notes in Computer Science. Berlin, Heidelberg: Springer Berlin Heidelberg, 2012. ISBN: 978-3-642-33867-0. DOI: 10.1007/978-3-642-33868-7.

[33] Garrett Birkhoff and Saunders Mac Lane. *A Brief Survey of Modern Algebra*. Macmillan, 1953, p. 276. URL: https://books.google.com/books/about/A{_}Brief{_}Survey{_}of{_}Modern{_}Algebra.html?id=SNlQAAAAMAAJ{\&}pgis=1.

[34] Y H Chen et al. “Parameter Estimation in Spherical Symmetry Groups”. English. In: *IEEE Signal Processing Letters* 22.8 (2015), pp. 1152–1155. ISSN: 1070-9908. DOI: 10.1109/LSP.2014.2387206. URL: http://ieeexplore.ieee.org/articleDetails.jsp?arnumber=7001052.

[35] U F Kocks, C N Tomé, and Hans-Rudolf Wenk. *Texture and anisotropy : preferred orientations in polycrystals and their effect on materials properties*. Cambridge University Press, 1998. ISBN: 0521465168 9780521465168.

[36] H.-J. Bunge. *Texture analysis in materials science : mathematical methods*. Butterworths, 1982. ISBN: 0408106425 : 9780408106429.

[37] S Gorelova, H Schaeben, and R Kawalla. “Quantifying texture evolution during hot rolling of magnesium Twin Roll Cast strip”. In: *Materials Science and Engineering: A* 602 (2014), pp. 134–142.

[38] T K Moon. “The expectation-maximization algorithm”. In: *Signal Processing Magazine, IEEE* 13.6 (1996), pp. 47–60.

[39] Mojtaba Ahmadieh Khanesar, Mohammad Teshnehlab, and Mahdi Aliyari Shoorehdeli. “A novel binary particle swarm optimization”. In: *Control & Automation, 2007. MED’07. Mediterranean Conference on*. IEEE. 2007, pp. 1–6.